

Multi-wavelength diffraction-limited imaging of the evolved carbon star IRC +10216, II

P. G. Tuthill¹, J. D. Monnier²,
and
W. C. Danchi³

ABSTRACT

High angular resolution images of IRC +10216 taken at various bandpasses within the near-infrared h , k & l bands are presented. The maps have the highest angular resolution yet recovered, and were reconstructed from interferometric measurements obtained at the Keck 1 telescope in 1997 December and 1998 April, forming a subset of a 7-epoch monitoring program presented earlier (Tuthill, Monnier, Danchi, & Lopez 2000, paper 1). Systematic changes with observing wavelength are found and discussed in context of present geometrical models for the circumstellar envelope. With these new high-resolution, multi-wavelength data and contemporaneous photometry, we also re-visit the hypothesis that the bright compact Core of the nebula (component “A”) marks the location of the central carbon star. We find that directly measured properties of the Core (angular size, flux density, color temperature) are consistent with a reddened carbon star photosphere (line-of-sight $\tau_{2.2} = 5.3$).

Subject headings: stars: individual(IRC +10216), stars: mass loss, techniques: interferometry

1. Introduction

IRC +10216 (= CW Leo) is a dusty, embedded carbon-rich long period variable presently undergoing an episode of intense mass-loss up to $10^{-5} M_{\odot}/\text{yr}$ (Mauron & Huggins 1999). It is the nearest object of its type (110-135 pc; Groenewegen 1997) and brightest in the thermal-IR, and is generally believed to be in transition between the latest stellar and the earliest planetary nebula phases. This fortuitous combination of factors has led to intensive study across the spectrum resulting in an extensive and rich literature, making IRC +10216 the textbook example for objects in its class. Although studies of molecular lines (eg. Biegging & Tafalla 1993) and deep imaging in

scattered galactic light (Mauron & Huggins 1999) reveal the outer parts of the mass-loss nebula to contain a series of spherical shells, the innermost regions show a bipolar structure (Kastner & Weintraub 1994). As the physical processes driving the transition from spherical to bipolar symmetry are not well understood, there has been much interest in imaging and modeling this system at the finest scales as a prototype addressing one of the outstanding problems in the latest stages of the stellar life cycle. The ability to recover diffraction-limited images in the infrared with a large-aperture telescope has delivered a detailed picture of the central regions of IRC +10216 (Haniff & Buscher 1998; Weigelt et al. 1998; Tuthill, Monnier, Danchi, & Lopez 2000; Osterbart et al. 2000; Weigelt et al. 2002). The bright Core is shown to be highly clumpy and inhomogeneous, and with studies now spanning some years, evolution of the material with apparent brightening, fading, and proper motion makes for considerable complexity in the immediate circumstellar environment. Here we present the highest angular res-

¹School of Physics, University of Sydney, NSW 2006, Australia

²University of Michigan at Ann Arbor, Department of Astronomy, 500 Church Street, Ann Arbor, MI 48109-1090, USA

³NASA Goddard Space Flight Center, Infrared Astrophysics, Code 685, Greenbelt, MD 20771, USA

olution images yet made, spanning the near infrared h , k , and l bands.

2. Observations

Using the techniques of aperture masking interferometry, images of IRC +10216 at a range of near-IR wavelengths were obtained from data taken at the 10 m Keck I telescope. These observations formed a somewhat distinct component of a program which also comprised the 7-epoch k band imaging study presented in Paper I. This paper is concerned with an intensive study of IRC +10216 made over only two observing runs in 1997 December and 1998 April, during which images were made in 5 separate near-infrared wavebands. The bandpasses of the filters used are given in Table 1 while an observing log showing the dates, aperture masks and filters can be found in Table 2.

In contrast to Paper I which was concerned with changes of the morphology of the dust shell between the separate epochs, here we have averaged together data taken over two separate runs. This was done to enhance the signal-to-noise (S/N) ratio of some of the maps, and to compensate for the fact that there was no single observing epoch which yielded high quality maps at all the observing wavelengths of interest. Although the two epochs chosen were only 4 months apart, measurable changes in the relative locations of components in the inner dust shell were shown to occur in Paper I. However, the fastest moving component would be displaced only ~ 8.5 mas in this interval (see Paper I) – averaging together maps with such small shifts should produce no great bias in the results.

The Golay and Annulus aperture geometries from Table 2 are described in detail in Tuthill et al. (2000b), which contains a thorough description of the experimental methods. Although the two masks employed did differ in performance for the various levels of source flux and seeing conditions encountered, comparisons proved that there were no systematic differences in the final maps produced allowing them to be averaged together by observing wavelength alone. As absolute positional information is not recovered from our closure-phase based techniques, maps to be averaged were registered with respect to each other by maximizing the cross-correlation before being

summed.

3. Results

This section presents the major observational findings of this paper. Diffraction-limited image reconstructions, visibility curves and additional supporting data are presented and discussed.

3.1. k band images – a comparison of bandwidths

Reconstructed images of IRC +10216 from data taken in 1997 December through two different filters, `kcont` and `ch4`, are given in Figure 1. As is apparent from Table 1, the `kcont` and `ch4` filters have similar central passbands, but their bandwidths differ by a factor of 3. The two images of Figure 1 do, however, exhibit a high degree of similarity to each other, with no significant departures beyond those to be expected at the lowest contours near the level of the noise. This is not surprising given that the emission process concerned is thermal radiation from warm dust which exhibits a fairly featureless spectrum across the near-infrared. The findings from this comparison, and other maps presented later in the paper, confirm that rapid changes in morphology with wavelength were not seen.

Images such as those of Figure 1 also present a useful yardstick for measuring the fidelity of the image reconstructions. The level of agreement shown is typical for maps taken with different aperture masks and on different nights with varying seeing conditions. Such external consistency checks have allowed us to determine that structures above a certain level, in this case about 3% of the peak, are very well established experimentally.

3.2. A descriptive model of IRC +10216

A qualitative model of the appearance of the dust shell around IRC +10216 was given in Paper I. We repeat this description here, together with a ‘cartoon sketch’ labeling the features given in Figure 2, which also gives the “A,B,C,D” nomenclature of Haniff & Buscher (1998). The brightest feature in the maps of Figure 1, appearing as a sharp spike at the map center, we denote as the Core (“A”). Surrounding the Core is a roughly elliptical region of emission elongated

TABLE 1
 PROPERTIES OF FILTERS

Name	Wavelength (μm)	Bandwidth (μm)
h	1.657	0.333
kcont	2.260	0.053
ch4	2.269	0.155
pahcs	3.083	0.101
pah	3.310	0.063

TABLE 2

JOURNAL OF INTERFEROMETRIC OBSERVATIONS. FOR CONSISTENCY WITH PAPER 1, WE HAVE PRESERVED THE NOMENCLATURE OF THE EPOCHS FROM THE LARGER 7-EPOCH SET PRESENTED EARLIER, EXPLAINING WHY THE EPOCHS START AT 2. SEE TEXT AND TABLE 1 FOR DESCRIPTIONS OF THE MASKS AND THE FILTERS.

Epoch	Date	Mask	Filters	Phase ¹
2	1997 Dec 16	Annulus	h,kcont	1.23
2	1997 Dec 16	Golay21	kcont,ch4,pahcs	1.23
2	1997 Dec 18	Golay21	kcont,pahcs,pah	1.23
3	1998 Apr 14	Golay21	ch4,pahcs	1.41
3	1998 Apr 15	Annulus	h,ch4,pahcs,pah	1.41

¹Stellar Phases from Monnier, Geballe & Danchi (1998)

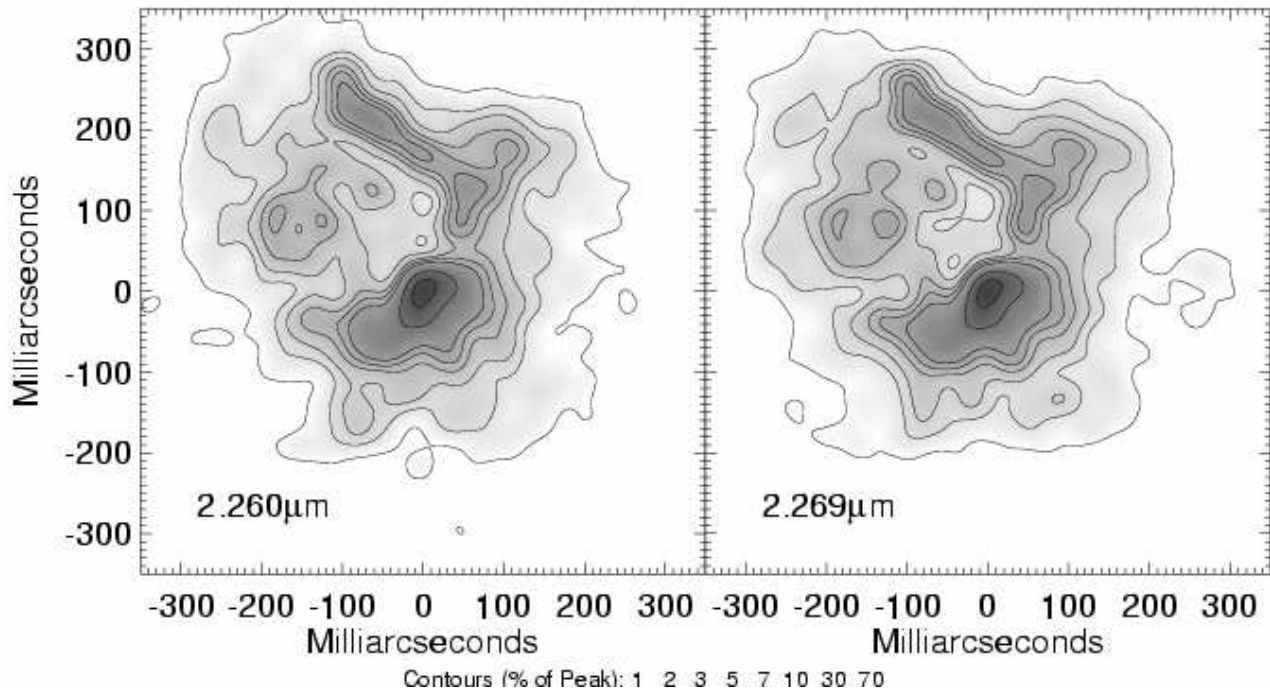


Fig. 1.— Image reconstructions of IRC +10216 in the near-infrared k band taken in 1997 December. *Left-hand panel* average of 4 maps taken with the kcont filter; *right-hand panel* average of 2 maps taken with the ch4 filter. See Table 1 for a description of filter properties.

along a position angle of $\sim 120^\circ$ which we label as the Southern Component. The shorter North Arm starts from a location 100 mas NW of the Core, and extends approximately 150 mas to the NNW (“C”). Perpendicular to it runs the prominent North-East Arm (“B”), running over 200 mas and forming the brightest structure outside the Southern Component. Displaced 150 mas from the Core to the NE is a region containing multiple weaker features, labeled as the Eastern Complex. Within this region, the brightest feature, which consists of a roughly circular patch somewhat less than 100 mas across, has been tagged as cloud EC1 (“D”). For further clarification of these assignments, see Figure 2 of Paper I. The different

nomenclature employed compared to other workers is necessitated by the higher angular resolution, so that the simple blobs reported in earlier work are resolved into clumpy or filamentary structures here.

3.3. Multi-wavelength near-infrared images

Maps of IRC +10216 spanning four near-infrared wavebands, representing a noise-weighted average of data collected over 1997 December and 1998 April are given in Figure 3. Unfortunately, the S/N and image fidelity was never as high for maps outside the k band. For shorter wavelengths,

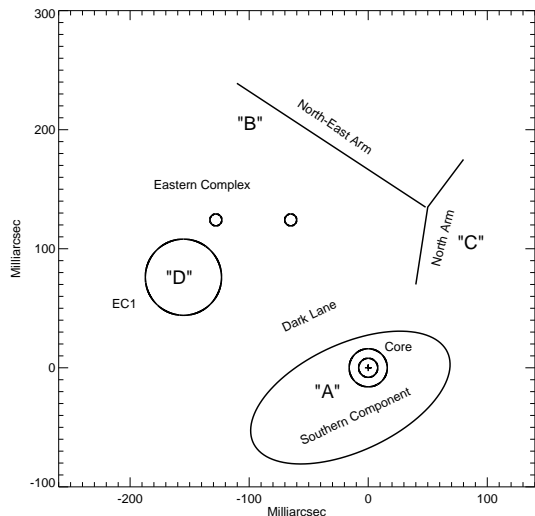


Fig. 2.— Cartoon diagram of features identified in high resolution images of IRC +10216 (see also Figure 2 from Paper 1). Features discussed in the text are labelled and registered against the peak of the bright Core of the Southern Component (denoted by the symbol + above). The “A,B,C,D” nomenclature of Haniff & Buscher (1998) is also indicated.

a combination of lower intrinsic flux from the star together with the greater role played by the atmospheric seeing were probably to blame for this loss. For the observations at wavelengths greater than $3\mu\text{m}$, the intrinsically lower system angular resolution probably contributed to enhanced difficulties with the mapping, although it is likely additional unidentified factors were also at play. For these reasons, the contour levels in Figure 3, chosen to be near or above the noise, are more conservative than for Figure 1. Despite this precaution, it can be seen for the map at $3.310\mu\text{m}$ (pah filter) resulting from an average of only two somewhat noisy maps, that the lowest contours do show the effects of noise.

In examining maps for systematic differences as a function of observing wavelength, the reader is cautioned to bear in mind that the four images of Figure 3 all have different angular resolutions and noise levels. Maps follow a similar basic shape, with the dominant features such as The Core, North and North-East Arms, and EC1 being identifiable at all wavelengths. However, it

is apparent that changes in appearance do occur across the near-infrared.

In order to visualize these changes, Figure 4 shows color maps produced by differencing the h-k and k-pahcs images. As might be expected in a source with such complexities of morphology where opacity, temperature and scattering all play varying roles, interpreting such maps is not straightforward. Of the bright high-SNR features, the Core exhibits the bluest (hottest) spectrum in k-pahcs. However, in the h-k map, this region exhibits a flat spectrum, neither relatively blue nor red, although the bluest feature in the map does lie quite nearby toward the dark lane. Even more puzzling is the behavior of the North/North-East Arm and (to a lesser extent) EC1, which are among the reddest features in the h-k map, yet appear markedly blue in k-pahcs. It is important to point out that among the many other physical properties which need to be modeled to understand these maps, there is also a strong molecular absorption feature due to HCN and C_2H_2 (Cernicharo et al. 1999) which coincides with the pahcs filter bandpass.

Further discussion of the colors and sizes of features, particularly the Core, is given later, however we prefer to do this based on simple models fit directly to the observed visibility data themselves. This is because the reconstruction of an image from a set of visibilities and closure phases is a complex and nonlinear process, and can be subject to biases introduced by the deconvolution process. Where possible, quantitative interpretation of the data is often best achieved by fitting to the measurements rather than proceeding by the intermediate step of a reconstructed image.

3.4. Visibility data

Simple quantitative brightness models were fit directly to the calibrated visibilities. Figure 5 presents azimuthally averaged visibility data for IRC +10216 at four near-infrared wavelengths. At all wavelengths, the visibility curves exhibit a common basic form. A rapid drop from high visibilities at the origin occurs over a spatial frequency range $\lesssim 0.5 \times 10^6 \text{ rad}^{-1}$, denoting that most of the flux comes from well-resolved large scale structure. This component has been modeled by fitting a circular Gaussian disk to the visibility data, the results of which are shown in Fig-

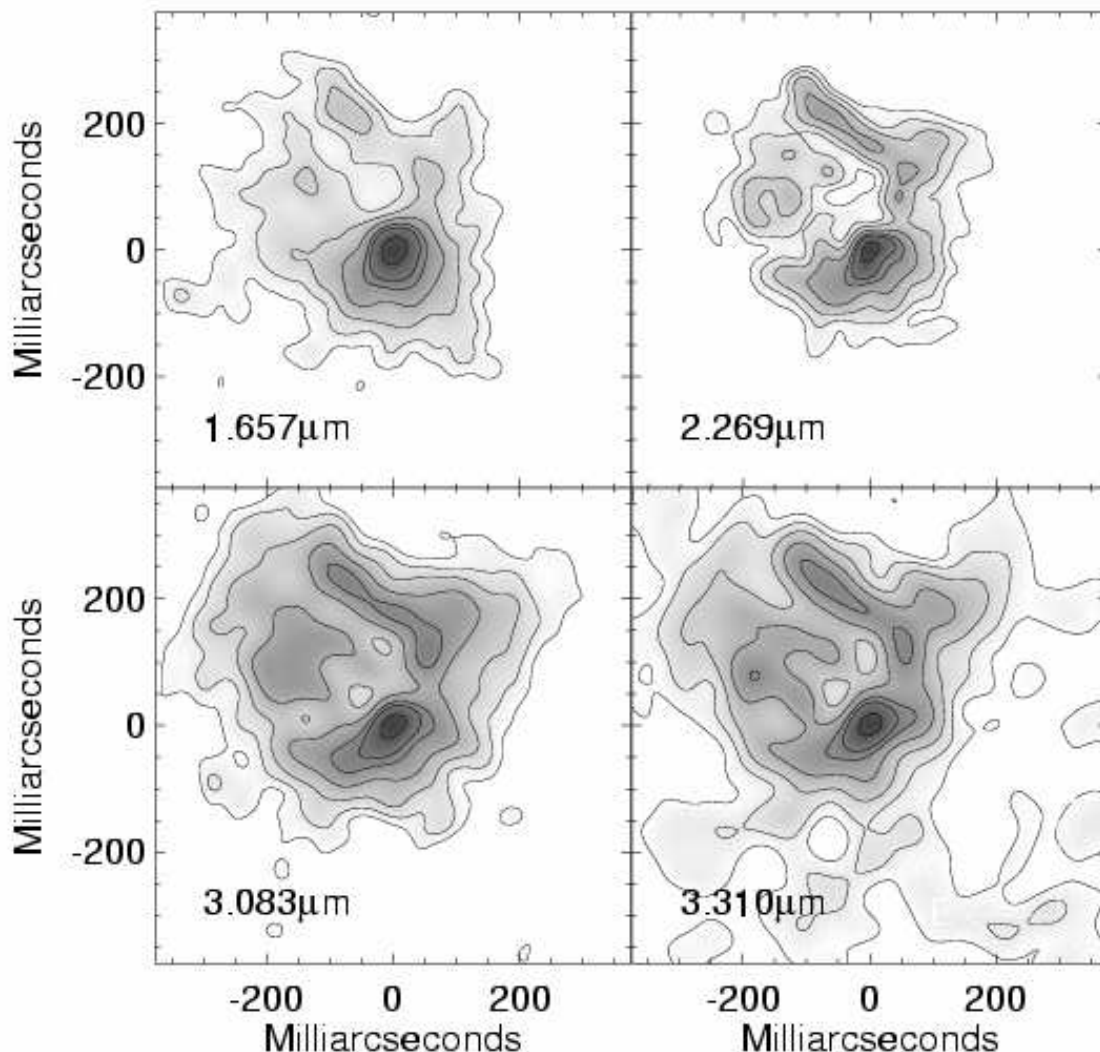


Fig. 3.— Image reconstructions of IRC +10216 from data taken at four different wavelengths in the near-infrared over the epochs 1997 December and 1998 January. *Upper left* average of 3 maps taken with the h filter; *upper right* average of 4 maps taken with the ch4 filter; *lower left* average of 8 maps taken with the pahcs filter; *lower right* average of 2 maps taken with the pah filter.

ure 5. Intermediate spatial frequencies ($0.5 \times 10^6 - 2.0 \times 10^6 \text{ rad}^{-1}$) carry much of the signal which results in the asymmetric form of the maps. Owing to this known complexity, no attempts were made to fit to azimuthally averaged visibilities on these intermediate baselines. At high angular resolutions ($\gtrsim 2.0 \times 10^6 \text{ rad}^{-1}$) visibilities for all wavelengths appear to follow a simple functional form

corresponding to a partially resolved, circularly symmetric, compact component. A uniform disk model has been fit to these data, and best fits are overplotted on the figure.

We proceed by identifying the uniform disk component fit to the long baselines as due to the Core. However, this identification requires careful argument and justification. The idea that

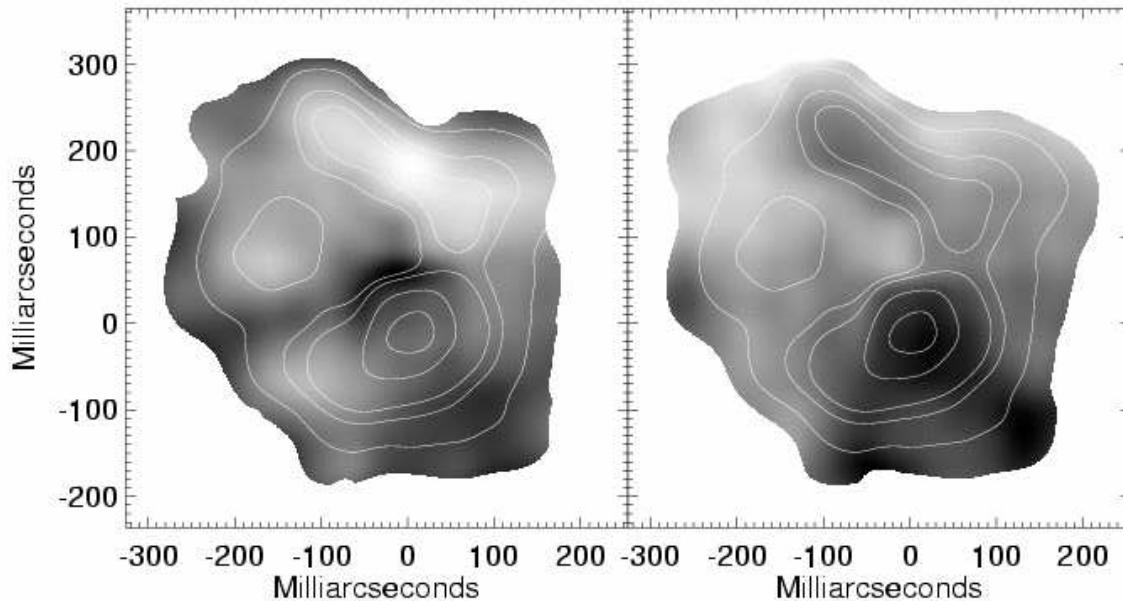


Fig. 4.— Color images with the $h - ch4$ filter (left panel) and the $ch4 - pahcs$ filter (right panel). In order to mitigate the effects of varying angular resolution for the different filters, images were smoothed to an effective beamsize of 70 mas before subtraction. Data were also truncated at 3% of the peak brightness giving rise to the blank areas at the edges. The overplotted contours show the structure from the smoothed $ch4$ map, indicating the locations of the Core and dominant features. For the $h - ch4$ map, the reddest (light) areas correspond to 3.7 mag, and the bluest (dark) 1.8 mag. For the $ch4 - pahcs$ map, the reddest areas are 3.0 mag and the bluest 1.4 mag. However, more extreme colors may occur over small regions but will be diluted by the smoothing mentioned above.

the Core is responsible for the highest spatial frequency structure is to an extent confirmed by the appearance of the recovered images, which show this to be by far the dominant compact feature. Furthermore, based on the physical assumption that the Core may indeed be the star, it is not unreasonable to expect that it is able to dominate the high-angular-frequency spectrum over flux coming from extended dust, which is less likely to have sharp structure on fine scales. In this case, mapping confirms the assumption to be reasonable, however there may be some non-core contamination of visibilities at intermediate baselines, a dif-

ficulty which only higher angular resolution can cure. A second important caveat concerns the high-resolution asymmetry noted to be associated with the Core (Tuthill, Monnier, Danchi, & Lopez 2000; Osterbart et al. 2000), which could cause difficulties in fitting to azimuthally averaged data (which assumes circular symmetry). The elongation was not as great at these epochs as it later became (Tuthill, Monnier, Danchi, & Lopez 2000), and tests were performed where data were grouped in sectors according to the orientation of the baseline. The spread of values found for these Core diameter fits was incorporated into the error term

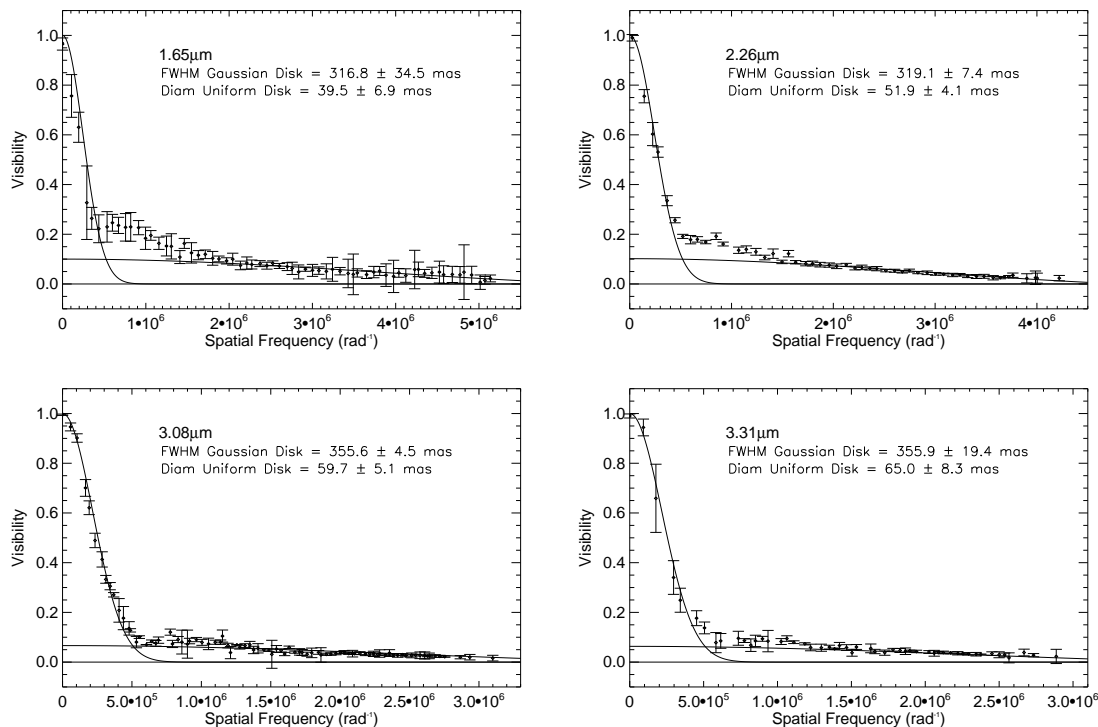


Fig. 5.— Azimuthally averaged visibility data for IRC +10216 at four different wavelengths: *Upper left* h filter; *upper right* ch4 filter; *lower left* pahcs filter; *lower right* pah filter. Two separate models (solid lines) have been fit to data over different spatial frequency ranges. The rapid fall-off in visibility at low resolution (spatial frequencies less than $4.5 \times 10^5 \text{ rad}^{-1}$ were used for the model) has been fit with a circular Gaussian disk model, with full-width at half-maximum (FWHM) given in the figure. The gradual decline at high spatial frequencies (greater than $2 \times 10^6 \text{ rad}^{-1}$ was used for the model), implying the presence of a bright partially-resolved component, has been fit with a uniform disk model with the diameter as given. Errors were computed from the spread of values among separate fits to a number of independent datasets at each wavelength. The best-fitting model parameters and their errors, together with the model visibility curves themselves, are all plotted in the figure.

for the final diameters given in Figure 5.

4. Discussion and Conclusions

The purported location of the stellar photosphere within the IRC +10216 nebula has been discussed in various studies starting with Kastner & Weintraub (1994). However, the complexities of the dust shell, and the absence of an unambiguously distinct bright compact component have caused continuing uncertainty over identifying which, if any, feature corresponds to the star itself. This has led to fundamental uncertainties over the structure of the dust shell, and determin-

ing the location of the star is essential to further progress. In Paper I we argued that the Core of the southern component (“A”) consisted of emission from the stellar photosphere with the possible addition of some flux from hot dust on the inner wall of a cavity or torus, tilted into the line of sight in the south. While this bright Core, with an angular diameter of 50 mas, was the prime candidate to be the stellar photosphere, the possibility that the star itself lay completely obscured behind the central dark dust lane was also advanced.

Osterbart et al. (2000) suggested an alternate interpretation, that the star itself lies within the bright knot at the end of the NE arm (compo-

nent “B”). Evidence supporting this view came from color maps, from observations of changes in shape of the Core, and particularly from attempts to trace the point of origin of the polarization field. An ambitious series of papers built on this interpretation, including detailed radiative transfer modeling (Men’shchikov et al. 2001; Men’shchikov, Hofmann, & Weigelt 2002) and the results of a further observational campaign (Weigelt et al. 2002). Detailed models interpreting the southern component as a cavity in a bipolar structure (“A”) with the star at the location of the North-East arm (“B”) were produced which gave reasonable fits to both the spectral energy distribution and the high resolution imaging. However these models were quite complex, incorporating >20 free parameters describing many different shells of varying symmetry and density profile. Based on this analysis, the authors rule out the possibility that the star can either be at the Southern Core, or that it was completely hidden behind the dust (Men’shchikov et al. 2001).

Despite this, there remain a number of simple arguments against the view that the star is located in the North-East arm. At the higher resolutions afforded by the Keck imaging, the North-East arm is seen to be a linear structure with almost uniform brightness along a ridge with no dominant compact knot. Furthermore, the North-East arm was found to be elongating and fading with time (Paper I), and in the most recent Keck observations (publication in preparation), almost absent entirely. Similar findings of the disappearance of the feature they previously identified as the star were explained by Men’shchikov, Hofmann, & Weigelt (2002) who invoke a recent and dramatic increase in mass-loss rate which has had the effect of burying it beneath a thickening dust shell. However our higher angular resolution Keck observations show that the North-East arm is actually lengthening and separating from the Southern Component, while it gradually fades out. The observed proper motion, with tentative acceleration detection (Tuthill et al. 2000b; Weigelt et al. 2002), would not be expected from the identifications of Men’shchikov et al. (2001) of these two components as a part of the circumstellar torus and the stellar photosphere.

Recent lunar occultation measurements (Chandrasekhar & Mondal 2001; Richichi, Chandrasekhar,

& Leinert 2003) have been able to shed some light on this question with extremely high angular resolutions (0.8 mas) attained in one-dimensional profiles. The Core of the southern component was found to be well fitted by a compact Gaussian profile with FWHM 35 mas contributing 6% of the total flux in k band. The close agreement with the expected angular size of the photosphere for the star, as well as the finding of a component of similar size and position in the h band profile, led these authors to identify the southern Core (“A”) as the stellar disk, although not with sufficient confidence to rule out alternative hypotheses.

By fitting only the longest baselines as shown in Figure 5, we were able to discriminate between the compact Core and the well-resolved nebula, revealing a partially-resolved component giving measurable visibility signal at even the longest baselines. For the four different bandpasses depicted (1.65, 2.26, 3.08 & 3.31 μm), uniform disk fits yielded diameters of 40, 52, 60 & 65 mas with relative flux contributions of 10, 10, 7 & 6% of the total respectively. Our k band uniform disk diameter of 52 mas is in close agreement with the lunar occultation measurements of Richichi, Chandrasekhar, & Leinert (2003) whose 35 mas FWHM Gaussian model would correspond, in the partially resolved case here, to a uniform disk diameter of 56 mas. The observed variation in angular diameter with wavelength across the near-IR is not necessarily strong evidence that the feature is a dust clump. To the contrary, it has become apparent that opacity changes due to various molecular and atomic species in the atmospheres of evolved stars lead to precisely such large apparent diameter variations, at least for M-stars (Tuthill et al. 2000a; Mennesson et al. 2002).

We turn now to examination of the apparent color of the compact Core. From the uniform disk fits above, the same relative contribution from the Core was found in h and k band (both 10%), but significantly less at the longer wavelengths (7 & 6% at 3.08 & 3.31 μm respectively). This finding is in good accord with the color maps presented in Figure 4 which found the Core to be neutral in h - k and blue in k - pahcs . If the Core is indeed the star, the simplest expectation is that the hottest effective temperature component of the system should present the bluest colors. The evidence here is somewhat equivocal: the Core is blue in k - pahcs ,

and adjacent to the bluest part of the h - k map, but clearly there are more complicated effects going on. To understand the color maps further, the complexities of scattering and reddening in an inhomogeneous environment must be more carefully modeled.

Lastly, we subject the hypothesis that component “A” is the stellar photosphere to a final quantitative test. Assuming the k band 52 mas Core is the stellar size, and if we adopt a reasonable effective temperature of 2000 K, the unreddened stellar flux density can be calculated. This flux density can be reddened by amorphous carbon dust (Rouleau & Martin 1991), and the resulting SED compared to the photometry of component “A” derived from the Keck aperture masking frames (calibrated using the contemporaneous interferometric calibrator and the visibility decomposition from Figure 5). Figure 6 shows the results of reddening the stellar spectrum with MRN dust (Mathis, Rumpl, & Nordsieck 1977) using the standard dust size range ($0.005\mu\text{m} < a < 0.25\mu\text{m}$), as calculated using DUSTY code (Ivezic et al. 1999). The k band flux density of “A” is well-fitted using $\tau_{2.2} = 5.3$, although the reddened spectrum is too red to fit the h band and L-band Core photometry. By including somewhat larger grains ($0.005\mu\text{m} < a < 0.75\mu\text{m}$), all the near-IR photometry of “A” is well-fitted (also, $\tau_{2.2} = 5.3$). This result is not sensitive to the adopted stellar effective temperature.

This simple test does not prove that component “A” is the star, however the hypothesis does gain credence. Furthermore, our results that $\tau_{2.2} = 5.3$ and the finding that the photosphere contributes 10% of k band emission is remarkably close to the estimate of Keady, Hall, & Ridgway (1988) who found $\tau_{2.2} = 5.4$ from SED modeling and a photospheric contribution $\sim 12\%$ confirmed by dilution of first-overtone CO absorption lines. Lastly, this line-of-sight dust absorption is consistent (within factor of two) with the mid-infrared *emission* modeled by Monnier et al. (2000), based on fits to the mid-IR spectrum and long-baseline interferometer (ISI) visibility data.

Although these arguments can certainly place the idea that component “A” is the star in a favorable light with respect to the known properties of the system, they cannot be turned around to rule out the alternate hypothesis that it is a dust

clump. The observed color temperature, given a number of plausible opacity and scattering geometries, could certainly fit with cool circumstellar material. Indeed, the finding that the Core is non-circular would seem to imply that at least some of the light arises from asymmetric circumstellar material, and/or that there are strong opacity gradients in the line of sight to the star.

In conclusion, although complicated models in which the star is obscured and eventually buried in the Northern regions cannot be ruled out, the simple alternate hypothesis that Core component “A” is highly-reddened, direct photospheric light can naturally explain the observed properties of the compact Core including: a) its angular size, b) its k band flux density, c) its color temperature, d) its persistence over multiple epochs, e) the observed dilution of near-IR photospheric absorption lines, f) the general level of mid-infrared emission, and g) the magnitude of proper motion between the Core and North-East arm (“A” and “B”). We encourage detailed radiative transfer modeling constrained by the latest multi-wavelength imaging to explore the physical structure of this fascinating source.

Devinder Sivia kindly provided the maximum entropy mapping program “VLBMEM”, which we have used to reconstruct our diffraction limited images. This work has been supported by grants from the National Science Foundation and the Australian Research Council. The data presented herein were obtained at the W.M. Keck Observatory, which is operated as a scientific partnership among the California Institute of Technology, the University of California and the National Aeronautics and Space Administration. The Observatory was made possible by the generous financial support of the W.M. Keck Foundation.

REFERENCES

- Bieging, J. H. & Tafalla, M. 1993, *AJ*, 105, 576
- Cernicharo, J., Yamamura, I., González-Alfonso, E., de Jong, T., Heras, A., Escribano, R., & Ortigoso, J. 1999, *ApJ*, 526, L41
- Chandrasekhar, T. & Mondal, S. 2001, *MNRAS*, 322, 356
- Groenewegen, M. A. T. 1997, *A&A*, 317, 503

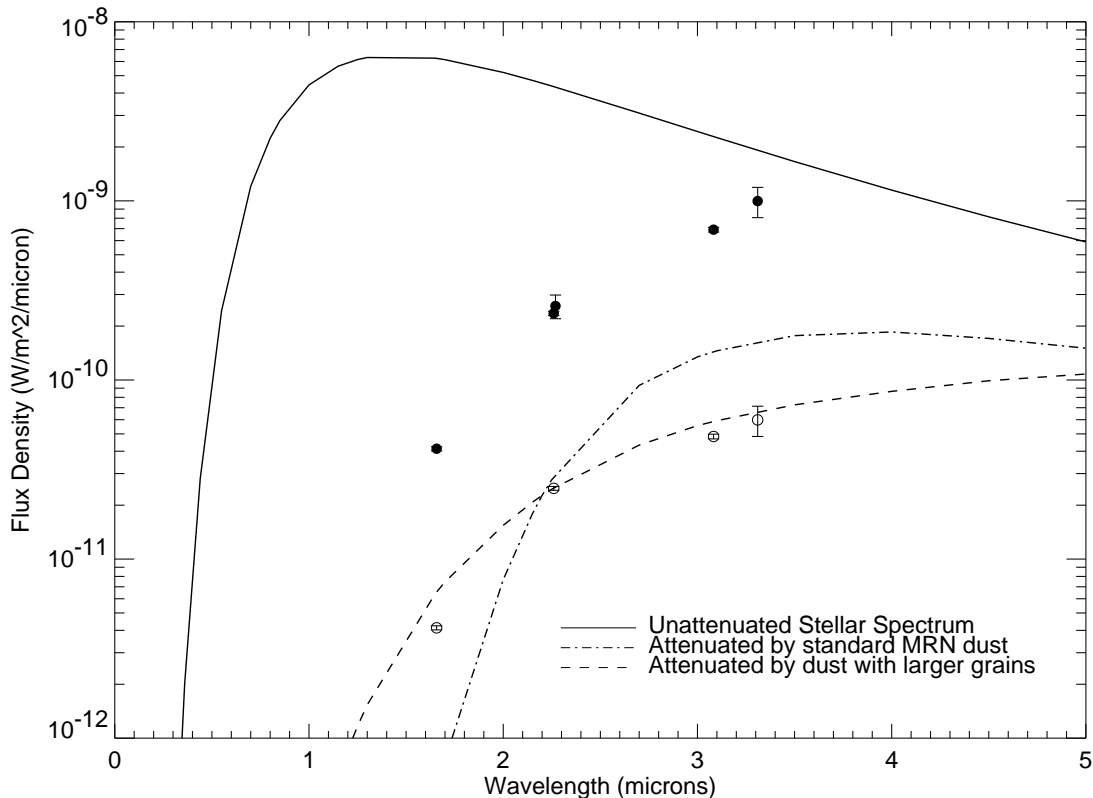


Fig. 6.— This figure shows the near-infrared spectral energy distribution of IRC +10216 as observed by the Keck aperture masking experiment in 1997 December (filled circles). The photometry of the bright compact Core (component “A”) was isolated from the surrounding nebula with high resolution techniques, and is also plotted (open circles). In addition to these data, a 2000K blackbody with uniform disk diameter 52 mas is shown (solid line). This stellar spectrum was reddened by standard MRN dust ($0.005\mu\text{m} < a < 0.25\mu\text{m}$, dot-dashed line) and MRN dust with larger grains ($0.005\mu\text{m} < a < 0.75\mu\text{m}$, dashed line), in both cases $\tau_{2.2} = 5.3$.

Haniff, C. A. & Buscher, D. F. 1998, *A&A*, 334, L5
 Ivezić, Z., Nenkova, M. & Elitzur, M., 1999, User Manual for DUSTY, University of Kentucky Internal Report
 Kastner, J. H. & Weintraub, D. A. 1994, *ApJ*, 434, 719
 Keady, J. J., Hall, D. N. B., & Ridgway, S. T. 1988, *ApJ*, 326, 832
 Mathis, J. S., Rumpl, W., & Nordsieck, K. H. 1977, *ApJ*, 217, 425
 Mauron, N. & Huggins, P. J. 1999, *A&A*, 349, 203

Mennesson, B., et al. 2002, *ApJ*, 579, 446
 Men’shchikov, A. B., Balega, Y., Blöcker, T., Osterbart, R., & Weigelt, G. 2001, *A&A*, 368, 497
 Men’shchikov, A. B., Hofmann, K.-H., & Weigelt, G. 2002, *A&A*, 392, 921
 Monnier, J.D., D., Geballe, T. R. & Danchi, W. C. 1998, *ApJ*, 502, 833
 Monnier, J. D., Danchi, W. C., Hale, D. S., Lipman, E. A., Tuthill, P. G., & Townes, C. H. 2000, *ApJ*, 543, 861
 Osterbart, R., Balega, Y. Y., Blöcker, T., Men’shchikov, A. B., & Weigelt, G. 2000, *A&A*, 357, 169

- Richichi, A., Chandrasekhar, T., & Leinert, C. 2003, *New Astronomy*, 8, 507
- Rouleau, F. & Martin, P. G. 1991, *ApJ*, 377, 526
- Tuthill, P. G., Monnier, J. D., Danchi, W. C., & Lopez, B. 2000, *ApJ*, 543, 284
- Tuthill, P. G., Danchi, W. C., Hale, D. S., Monnier, J. D., & Townes, C. H. 2000a, *ApJ*, 534, 907
- Tuthill, P. G., Monnier, J. D., Danchi, W. C., Wishnow, E. H., & Haniff, C. A. 2000b, *PASP*, 112, 555
- Weigelt, G., Balega, Y., Bloeker, T., Fleischer, A. J., Osterbart, R., & Winters, J. M. 1998, *A&A*, 333, L51
- Weigelt, G., Balega, Y. Y., Blöcker, T., Hofmann, K.-H., Men'shchikov, A. B., & Winters, J. M. 2002, *A&A*, 392, 131